Applied Catalysis B: Environmental 341 (2024) 123298

Contents lists available at ScienceDirect

Applied Catalysis B: Environmental

journal homepage: www.elsevier.com/locate/apcatb

Ionomer-free nanoporous iridium nanosheet electrodes with boosted performance and catalyst utilization for high-efficiency water electrolyzers

Zhiqiang Xie [a,1], Lei Ding [a,1], Shule Yu [a,1], Weitian Wang [a], Christopher B. Capuano [b], Alex Keane [b], Kathy Ayers [b], David A. Cullen [c], Harry M. Meyer III [d], Feng-Yuan Zhang [a,*]

[a] Nanodynamics and High-Efficiency Lab for Propulsion and Power, Department of Mechanical, Aerospace & Biomedical Engineering, UT Space Institute, University of Tennessee, Knoxville, Tullahoma, TN 37388, USA
[b] Nel Hydrogen, Wallingford, CT 06492, USA
[c] Center for Nanophase Materials Sciences, Oak Ridge National Laboratory, Oak Ridge, TN 37831, USA
[d] Chemical Sciences Division, Oak Ridge National Laboratory, Oak Ridge, TN 37831, USA

ARTICLE INFO

Keywords:
Green hydrogen production
Nanoporous iridium nanosheets
Thin titanium liquid/gas diffusion layers
Low catalyst loading
PEM water electrolysis

ABSTRACT

Increasing the catalyst utilization efficiency and simplifying electrode fabrication processes are crucial to accelerate development of low-cost proton exchange membrane electrolyzer cells (PEMECs). Here, we develop a facile route to fabricate ionomer-free iridium nanosheet integrated electrodes, in which nanoporous iridium nanosheets (IrNS) with abundant exposed edges and nanopores are deposited on thin titanium liquid/gas diffusion layers (TT-LGDLs) via a low-temperature chemical synthesis strategy. Benefiting from high catalytic activity, good electrode conductivity and excellent liquid/gas transport properties, such nanoporous IrNS electrodes with low catalyst loadings require low cell voltages of 1.65 V and 1.78 V at 3000 and 6000 mA/cm^2, respectively. More impressively, a stable performance can be well maintained under extremely high current density tests of 5000 mA/cm^2, demonstrating the potential of low-loading nanoporous IrNS electrodes in solid-electrolyte based electrochemical conversion cells that require high current density operation.

1. Introduction

The climate change and global decarbonization is deriving the urgent demand for clean energy conversion and storage technologies [1–6]. The proton exchange membrane electrolyzer cell (PEMEC) has emerged as a very promising energy storage technology for hydrogen production from water electrolysis when integrated with solar, wind and other renewable energy sources [2,3,7–9]. Compared with conventional water electrolyzer systems, PEMECs have many unique advantages, including high efficiency, quick startup, compact design, low maintenance cost, and close-to-zero emissions. The membrane electrode assembly (MEA) is very important to the overall cell performance and cost of the PEMEC. To achieve high efficiency and long durability of a PEMEC, high loadings of platinum-group metals (2–3.0 mg_{Ir}/cm^2) are generally required for the oxygen evolution reaction (OER) [5,10–13].

Currently, the catalyst-coated membrane (CCM) and catalyst-coated porous transport layer as gas diffusion electrode (GDE) are two main electrode designs in PEMECs. Nafion ionomers are commonly applied in anode and cathode catalyst layers (CLs) for both CCM and GDE designs. The Nafion ionomer in CLs not only serves as proton conductors to promote proton transport from membrane to the catalyst surface and to extend the electrode/electrolyte reaction zone, but also function as the binder to physically stabilize the catalysts on the membrane. For the CCM design, Bernt et al. investigated the impact of ionomer content in anode CLs on cell performances and reported that 11.6 wt% ionomer in IrO_2/TiO_2 anode CLs showed the best cell performance among the tested anodes with an ionomer content from 2.2 to 28 wt% [14]. Kulkarni et al. fabricated ionomer-containing CCMs and GDEs, and compared their cell performances at different catalyst loadings [15]. They found that the ionomer in CLs hinders the catalyst utilization efficiency to some extent in both cases.

Recent studies have demonstrated advantages of ionomer-free electrode designs over conventional ionomer-containing electrodes, including improvement of catalyst utilization efficiency, energy efficiency enhancement, stability and remarkably simplified electrode fabrication steps [16–22]. For example, Sapountzi et al. fabricated CCMs

* Corresponding author.
E-mail address: fzhang@utk.edu (F.-Y. Zhang).
[1] These authors contributed equally to this work.

https://doi.org/10.1016/j.apcatb.2023.123298
Received 8 May 2023; Received in revised form 31 August 2023; Accepted 14 September 2023
Available online 16 September 2023

with ionomer-free IrO_x and Pt catalyst layers at anode and cathode via a spark ablation process [16]. Such ionomer-free CCMs with low catalyst loadings (0.8 mg_{Ir}/cm^2, 0.5 mg_{Pt}/cm^2) demonstrated significantly improved cell performance compared to conventional ionomer-containing CCMs (2 mg_{IrRuOx}/cm^2 at anode, 4 mg_{Pt}/cm^2 at cathode). More recently, Higashi et al. fabricated ionomer-free IrO_2 nanostructured textile based CCMs by the combination of electrospun PVP textiles and subsequent magnetron radiofrequency (RF) sputtering of IrO_2 catalysts and hot-pressing transfer to Nafion 212 membrane [17]. The cell performances at low loading levels of 0.1–0.3 mg_{Ir}/cm^2 are superior to ionomer-containing electrodes with the similar loadings. However, complicated CCM fabrication process and involvement of expensive electrospinning, sputtering and hot press equipment would limit the scale-up manufacturing, especially for large-size samples. Choe et al. reported an ionomer-free GDE design composed of electrodeposited IrO_2 catalysts on the Ti mesh substrate (0.4 mg/cm^2), and demonstrated a higher current density of 0.97 A/cm^2 at 1.6 V and improved stability compared to ionomer-containing IrO_2 GDE [18]. Lim et al. fabricated ionomer-free Pt@IrO_2 core-shell structured anodes by using sequential electrodeposition of 0.27 mg_{Pt}/cm^2 hemispherical Pt particles as support and 0.16 mg_{Ir}/cm^2 IrO_2 as catalysts on the Ti felt substrate [19]. This electrode with the total precious metal loading of 0.43 mg/cm^2 displayed enhanced cell performances than electrodeposited IrO_2 anode without Pt support.

To further enhance the catalyst utilization and performance of ionomer-free electrode designs, engineering nanostructures and tuning compositions of catalyst layers as well as electrode patterns have been explored [15,17–19,21,23–28]. Nevertheless, the cell performance and durability of most previously reported OER electrodes at high current densities are still far from satisfactory for real applications. Therefore, there is a continuing need to optimize the electrolyzer electrode design with minimal catalyst use, and meanwhile to further improve energy efficiency and durability in harsh acidic and oxidizing conditions.

In this study, we report a simple process to prepare ionomer-free iridium nanosheet electrodes, in which nanoporous iridium nanosheets (IrNS) with abundant exposed edges and nanopores are deposited on thin titanium liquid/gas diffusion layers (TT-LGDLs). Different from other reported electrolyzer electrodes in the literature, the nanoporous IrNS electrode has the following unique advantages: (1) Multifunctional TT-LGDLs can minimize ohmic and mass transport losses as compared to conventional 3D porous transport layers (PTLs); (2) The ionomer-free nanoporous iridium catalyst layer can provide abundant reaction sites for electrochemical reactions and significantly reduce the reaction overpotentials or activation losses in a PEMEC. (3) The required loading of catalysts can be greatly reduced from several mg/cm^2 down to 0.3 mg/cm^2 or lower, thus decreasing the catalyst material cost. (4) The whole electrode fabrication and assembly are simplified compared to conventional electrodes (CCM/LGDLs) with multi-step and complicated fabrication processes. Thanks to the above-mentioned benefits, nanoporous IrNS electrodes with low catalyst loadings can deliver the current densities of 2000 mA/cm^2 at a low cell voltage of 1.78 V when coupled with Nafion 117 (~ 175 μm), showing a about 10 times higher mass specific current than that of the conventional CCM baseline. More impressively, when coupled with Nafion 212 (~ 50 μm), a higher current density of 6000 mA/cm^2 can be achieved at the low cell voltage of 1.78 V. The stable cell performances are demonstrated for both Nafion 117 and Nafion 212 cases at high current densities, indicating the great potential for the application of nanoporous IrNS electrodes in the practical PEMECs under the high current density operation. The whole electrode design in this work can also be generalized to other solid-electrolyte based electrochemical conversion cells that require high current density operation.

2. Experimental section

2.1. Fabrication of ionomer-free IrNS integrated electrodes

TT-LGDLs with distributed circular pores were manufactured by wet etching of titanium foils with the assistance of lithographically-pattered resist masks [29]. TT-LGDLs were surface cleaned by acetone, ethanol and deionized (DI) water with sonication for 15 min. Afterwards, oxalic acid (OA) treatment was performed to remove the native titanium oxide layer from LGDL substrates. The LGDL substrates were completely immersed into the reaction solution containing 1 mL 40 mM $IrCl_3$ solution (Sigma-Aldrich), 1 mL dimethylformamide (DMF) (Sigma-Aldrich), 1 mL DI water, 1 mL formic acid (Sigma-Aldrich), and 5 mg of poly(ethylene oxide)-b-polystyrene (PEO-b-PS, Polymer Source Inc). The reaction solution was heated at 80 °C for 5 h and cooled down to room temperature. Finally, the IrNS was deposited on the surface of LGDL substrates, forming the nanoporous IrNS electrode. After post-washing with acetone and ethanol for at least three times, the nanoporous IrNS electrode was annealed at 150 °C for 15 min in vacuum for sample characterizations and cell performance testing. The catalyst loadings were achieved and determined by measuring the mass difference before and after the IrNS deposition on the employed LGDL substrate. Afterwards, based on the wetted surface area of the substrate, the catalyst loading is calculated.

2.2. Materials characterization

The surface morphology and chemical composition of nanoporous IrNS electrodes were characterized by a field emission scanning electron microscope (SEM) (JSM-IT700HR), which is equipped with energy-dispersive X-ray spectroscopy (EDS). The nanostructure of IrNS catalysts was characterized by aberration-corrected scanning transmission electron microscopy (STEM) on a JEOL JEM-ARM200F "NEOARM" operated at an acceleration voltage of 80 kV. A Rigaku SmartLab X-ray diffraction (XRD) system was used to investigate the crystalline structure of the sample. The X-ray photoelectron spectroscopy (XPS) analysis was performed to identify the surface chemistry of samples on a Thermo Scientific K-Alpha spectrometer.

2.3. Electrochemical measurements

The as-synthesized IrNS catalysts on Ti substrate, a graphite rod counter electrode, and a Ag/AgCl reference electrode were used in a three-electrode system with the liquid electrolyte of 0.5 M H_2SO_4. The linear sweep voltammetry (LSV) curves were measured by a Potentiostat (VSP/VMP3B-100, Bio-Logic) at a scan rate of 5 mV/s at room temperature.

2.4. Cell assembly and performance evaluation of the PEMEC

A carbon paper (Toray 090) (280 μm in thickness, 78% porosity) was used as the cathode LGDL. The grade 2 Ti-made bipolar plate and graphite-made bipolar plate (AXF-5Q) with parallel flow channels were used at anode and cathode, respectively. The nanoporous IrNS electrode, single-sided CCM, and carbon paper, together with the gaskets and the bipolar plates were sandwiched by two stainless steel end-plates to assemble a PEMEC. Afterwards, the PEMEC was compressed by eight evenly distributed ¼ 20 bolts, which were tightened to a torque of 40 lb-in. A schematic illustration of electrode assembly in a PEM water electrolyzer is shown in Fig. S1. All the cell tests were conducted in a PEMEC with a 5 cm^2 active area. A temperature of 80 °C, atmospheric pressure, and a water flow rate of 20 mL/min at anode were used for all cell tests. The commercial cathode-only single-sided CCMs with the Pt black (1.0 mg_{Pt}/cm^2) at cathode and Nafion 117 with a thickness of 175 μm, and the commercial two-sided CCMs with 2.0 mg_{Ir}/cm^2 IrO_x at the anode, 1.0 mg_{Pt}/cm^2 Pt black at the cathode and N117 membrane as the

baseline were supplied by Nel. The Pt/C (0.14 mg_{Pt}/cm^2) at cathode and Nafion 212 with a thickness of ~ 50 μm serving as the electrolyte were home-made by a direct spray coating process, based on the modified recipe in our previous publication [30]. The polarization curves were collected by a Potentiostat (VSP/VMP3B-100, Bio-Logic). The electrochemical impedance spectroscopy (EIS) plots were recorded from 10 kHz to 50 mHz at 1000 mA/cm^2. The high-frequency resistance (HFR) refers to the ohmic resistance value obtained at high frequencies, which is used to indicate the total ohmic resistance of the PEM electrolyzer cell. The HFR plots were recorded under the high frequency of ~ 3 kHz by using the Staircase Galvano Electrochemical Impedance Spectroscopy (SGEIS) technique with Biologic EC-Lab software. HFR correction is conducted by using the mean HFR values and current density densities to calculate the HFR-free cell voltages according to the following equation: $V_{HFR\text{-}free} = V_{cell} - I \bullet HFR$. With the help of HFR-correction, the activation losses between the IrNS electrode and CCM baseline in the PEMECs can be directly compared.

3. Results and discussions

3.1. Morphology and crystal structure of nanoporous IrNS electrode

The schematic in Fig. 1 illustrates the cost-effective and facile fabrication of the nanoporous IrNS integrated electrode via a low-temperature chemical synthesis approach. The microstructures (e.g., pore size, porosity, etc.) of the TT-LGDL substrate have been systematically studied and optimized in our previous research. For instance, the TT-LGDL with the pore size of 100 μm and thickness of 25 μm exhibited over 9% energy efficiency enhancement at 2000 mA/cm^2 and enhanced mass transport properties compared to conventional 350-μm-thick Ti felt LGDLs [29]. Moreover, with the same porosity, the TT-LGDL with the pore size of 100 μm displayed smaller activation and mass transport losses than TT-LGDLs with larger pore sizes of 200 and 300 μm [20]. As a proof of concept, we selected the TT-LGDL with ~ 100 μm pore size and ~ 40% porosity as the substrate for deposition of the IrNS on TT-LGDLs in this study. The surface-treated TT-LGDL substrates were completely immersed into the reaction solution and kept at 80 °C for 5 h to obtain the nanoporous IrNS electrode, in which IrNS was deposited on the modified TT-LGDL substrates. During the synthesis process, the reducing agent of formic acid (HCOOH) undergoes decomposition and generates the carbon monoxide (CO) molecules. Previous studies have demonstrated that CO is capable of strongly binding to the specific crystal facets of diverse catalytic metals (e.g., Ir, Pd, etc.), facilitating the two-dimensional (2D) nanosheet formation [31,32]. With the help of block polymer PEO-*b*-PS template, Ir nanocrystals nucleate and grow into 2D Ir nanosheets with numerous nanopores. In addition to the nanopore formation on the basal planes of Ir nanosheets, the secondary porous structure with large pores is also constructed among individual nanosheets during the continuous growth process.

Different nanoporous IrNS catalyst loadings can be achieved by merely adjusting the iridium precursor concentrations under the same reaction time and temperature. Based on our experimental results, the minimum concentration of the Ir chemical precursor ($IrCl_3$) of at least 40 mM is required for successful and relatively uniform deposition of IrNS on the LGDL substrate. The amount of iridium loss during the deposition process is about 10%. Increasing the Ir concentration would result in the IrNS loading increase on the employed LGDL substrate without altering the nanostructures of IrNS catalysts. Conversely, when the $IrCl_3$ concentration is lower than 40 mM, the deposition of IrNS catalysts on the LGDL substrate becomes non-uniform. Our research work is still ongoing to obtain a better understanding of IrNS deposition mechanism on the LGDL substrate.

The morphology, nanostructure and elemental composition of the nanoporous IrNS integrated electrode were first characterized by SEM and EDS techniques. As shown in Figs. 2a-2c the applied TT-LGDL substrate in this study shows relative smooth surface and well-defined circular pore morphology with the average pore size of ~ 100 μm, calculated porosity of ~ 40% and ~ 25 μm in thickness. The high-resolution SEM images in Figs. 2d-f reveal that nanoporous IrNS catalysts with abundant exposed active edges were successfully deposited on a surface-treated TT-LGDL substrate with a full surface coverage and good uniformity. The SEM images and corresponding EDS maps in Figs. 2g-2i and Fig. S2 show the relatively homogenous elemental distribution of Ir across the entire nanoporous IrNS integrated electrode, further confirming the uniform surface coverage of IrNS on the TT-LGDL substrate. To study the crystal structure of as-synthesized nanoporous IrNS catalysts, the catalysts and the underlying substrate were separated by sonication and then the catalysts were collected for the XRD measurement. The XRD pattern in Fig. 2j indicates that as-synthesized nanoporous IrNS catalysts are polycrystalline and composed of metallic Ir with the fcc crystal structure, which matches well with the standard XRD pattern of Ir fcc (JCPDS No.: 06–0598). There are no detected secondary impurity phases or oxidized Ir phase in the sample. The metallic IrNS is expected to give rise to better conductivity of the

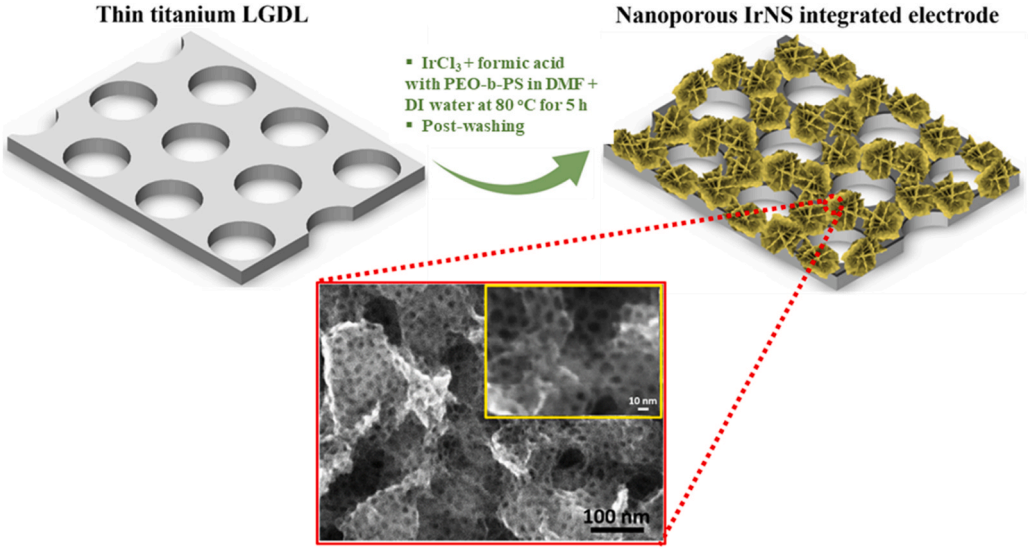

Fig. 1. Schematic illustrating the design of the nanoporous IrNS integrated electrode composed of in-situ deposited ultrathin nanoporous iridium nanosheets on thin titanium LGDLs via a low-temperature chemical synthesis strategy.

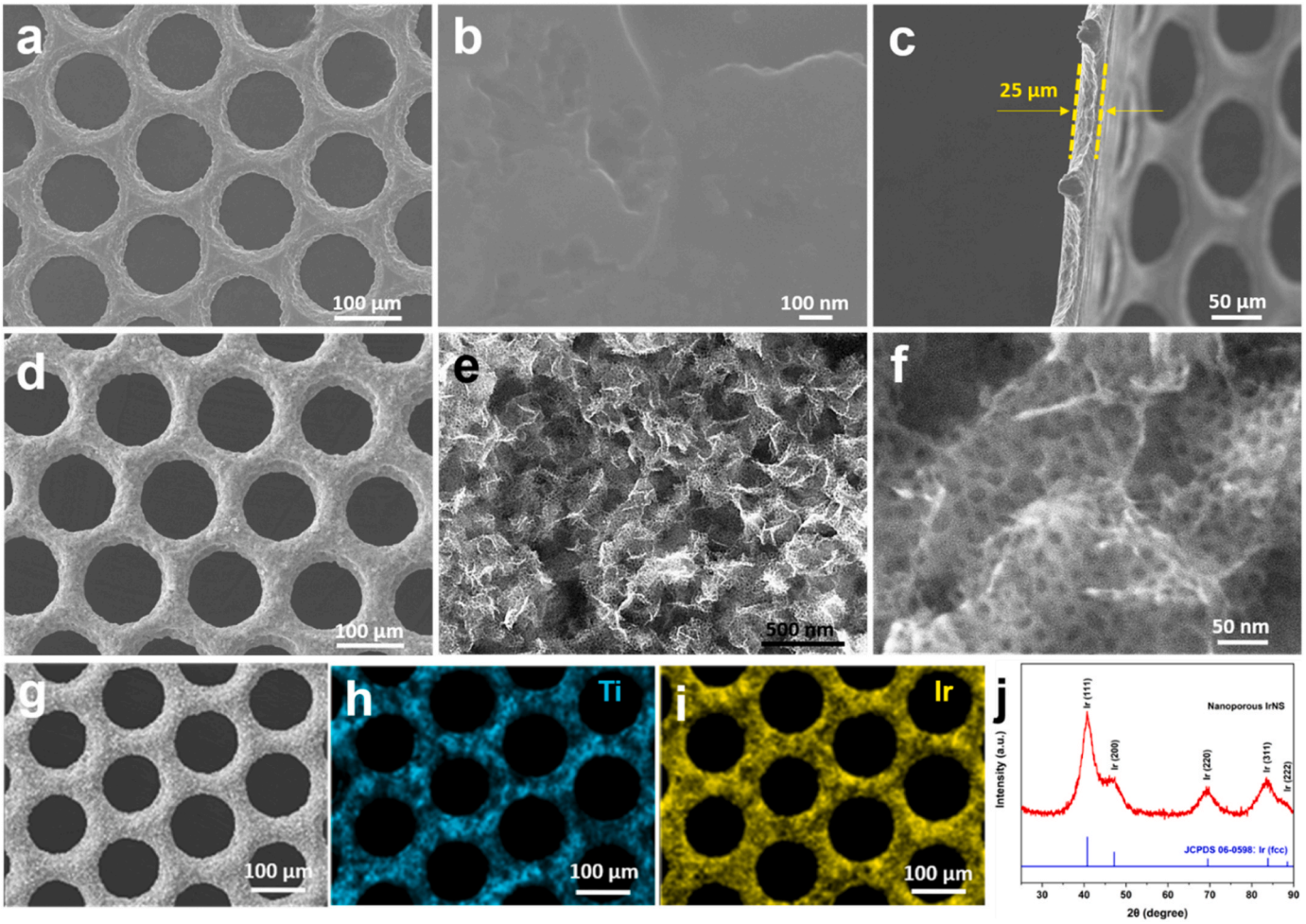

Fig. 2. Morphological and compositional characterizations. (a-b) Top-view and (c) cross-section SEM images of the employed TT-LGDL substrate. (d-f) SEM images of the nanoporous IrNS integrated electrode. (g-i) SEM-EDS elemental mapping of the electrode. (j) XRD pattern of the nanoporous IrNS catalysts.

entire catalyst layers than other iridium oxide based catalysts. More importantly, the elimination of ionomer in the catalyst layer would also greatly reduce the ohmic resistance of the electrodes in practical PEMECs, especially compared to most commonly used ionomer-mixed catalyst layers. Collectively, the above SEM, EDS and XRD characterization results demonstrate the successful fabrication of ionomer-free nanoporous IrNS integrated electrodes with desirable nanostructure, good surface coverage and uniformity as well as the dominant metallic IrNS.

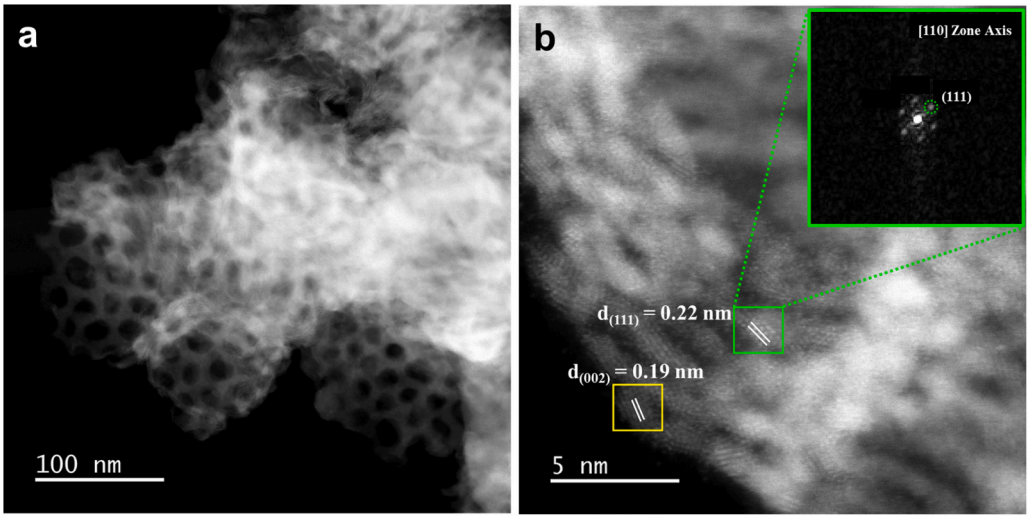

Fig. 3. (a-b) HAADF-STEM images of as-synthesized IrNS catalysts prior to cell test in PEMECs.

3.2. Nanostructure of nanoporous IrNS catalysts

To obtain more detailed structural information, high-angle annular dark-field (HAADF)-STEM images of as-synthesized IrNS catalysts were obtained. As seen from STEM images in Fig. 3a, nanopores are formed within the individual nanosheets. The measured lattice fringes in Fig. 3b are 0.19 and 0.22 nm, corresponding to (002) and (111) planes of the metallic iridium with a fcc crystal structure. The inset in Fig. 3b shows the fast Fourier transform (FFT) pattern calculated from the corresponding green box, further confirming the (111) crystal plane for the metallic iridium.

3.3. Full cell characterization of nanoporous IrNS in PEMECs with N117 membrane

Prior to the full cell characterization in PEMECs, the intrinsic activity of nanoporous IrNS catalysts for the OER was first evaluated in a half electrochemical cell. As shown in Fig. S3, the nanoporous IrNS electrode displays a low overpotential of 270 mV at 10 mA/cm^2 and small Tafel slope of 53 mV/dec, outperforming benchmarking IrO_2 nanoparticles

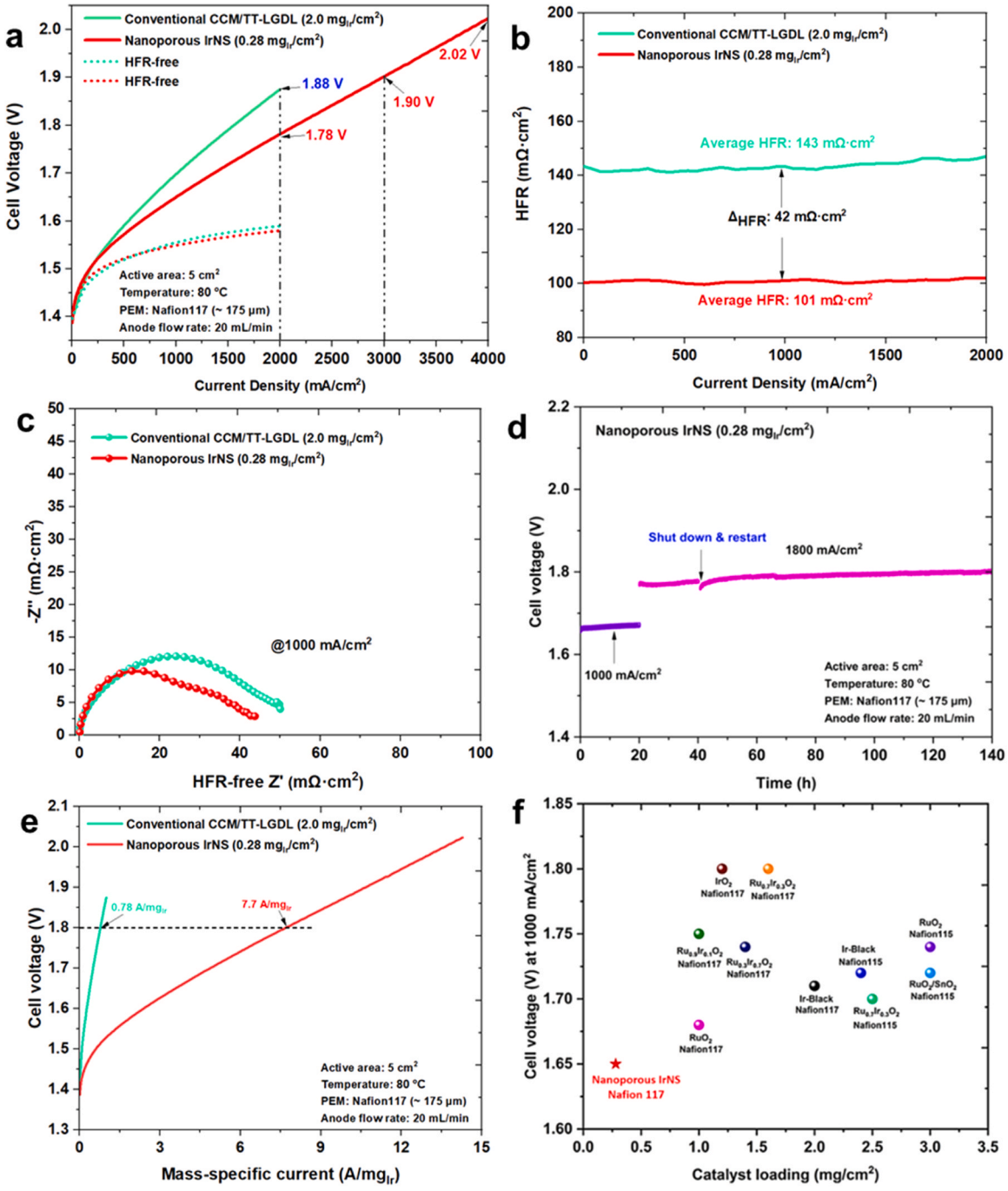

Fig. 4. (a) Polarization curves of a nanoporous IrNS integrated electrode (0.28 mg$_{Ir}$/cm^2) coupled with Nafion 117 membrane and conventional CCM/TT-LGDL baseline in PEMECs at 80 °C. (b) The high-frequency resistance (HFR) comparison between 0 and 2000 mA/cm^2. (c) The HFR-free EIS plots of nanoporous IrNS (0.28 mg$_{Ir}$/cm^2) and conventional CCM/TT-LGDL baseline at 1000 mA/cm^2. (d) Cell stability test at 1000 mA/cm^2 for initial 20 h and subsequent test at 1800 mA/cm^2 for over 120 h. (e) Mass-specific current comparison. (f) Cell performance comparison of nanoporous IrNS integrated electrodes with previously reported Ir and Ru-based OER electrodes at 1000 mA/cm^2 in the literature.

and other Ir-based OER catalysts in the literatures [40,55]. The nanosheet structure and nanopores in the individual nanosheets can expose abundant active sites, leading to improved OER performance. When coupled with Nafion 117 (~ 175 μm), the polarization curves in Fig. 4a show that the nanoporous IrNS electrode with a low catalyst loading of 0.28 mg_{Ir}/cm^2 can deliver the current densities of 1000, 2000, 3000 and 4000 mA/cm^2 at low cell voltages of 1.65, 1.78, 1.90 and 2.02 V, respectively. On the contrary, the conventional CCM/TT-LGDL baseline with a high loading of 2.0 mg_{Ir}/cm^2 requires a higher cell voltage of 1.88 V at 2000 mA/cm^2, which is much larger than the nanoporous IrNS electrode by 100 mV. After high-frequency resistance (HFR) correction, nanoporous IrNS electrode displays about 10 mV activation loss reduction in comparison with the high-loaded CCM/TT-LGDL baseline, indicating boosted catalyst utilization with the newly developed nanoporous IrNS electrode design. Furthermore, large ohmic loss generally occurs in PEMECs with the conventional ionomer-mixed MEA, owing to the low conductivity of the entire catalyst layers. For instance, as shown in Fig. 4b, the CCM/TT-LGDL baseline exhibits a high average HFR value of 143 $m\Omega*cm^2$ at 80 °C. However, benefiting from the ionomer-free IrNS catalyst layer, the nanoporous IrNS electrode shows an average HFR value of as small as 101 $m\Omega*cm^2$, which is about 42 $m\Omega*cm^2$ smaller than the baseline, which are consistent with the EIS results in Fig. S4. Such large HFR reduction results in about 84 mV improvement of the overall cell performance at 2000 mA/cm^2. The HFR-free EIS analysis at 1000 mA/cm^2 in Fig. 4c shows that the PEMEC with nanoporous IrNS electrode has smaller activation and mass transport losses in total than the CCM/TT-LGDL baseline, as evidenced by the smaller size of semi-arch than the CCM/TT-LGDL baseline. This result implies that the ionomer-free nanoporous IrNS electrode could facilitate the electron transfer across the entire catalyst layer, superior to conventional ionomer-mixed catalyst layers in the CCM-based PEMECs.

To validate the electrode stability in PEMECs, the stability test of nanoporous IrNS electrodes under a high current density of 1800 mA/cm^2 was conducted. As seen from Fig. 4d, after the initial 20-h test at 1000 mA/cm^2, the cell voltage slightly increases from ~ 1.762–1.802 V during the subsequent 120-h test at 1800 mA/cm^2, displaying a small performance degradation rate of 0.33 mV/h. To compare the catalyst utilization levels, the mass-specific current plots are derived by normalizing the delivered current to mass for nanoporous IrNS integrated electrode (0.28 mg_{Ir}/cm^2) and conventional CCM/TT-LGDL baseline, as shown in Fig. 4e. By comparison, the mass-specific current of nanoporous IrNS integrated electrode is as high as 7.7 A/mg_{Ir} at the cell voltage of 1.8 V, which is about 10 times higher than the CCM/TT-LGDL baseline. This mass-specific current comparison demonstrates that boosted catalyst utilization and performance can be achieved by adopting ionomer-free nanoporous IrNS integrated electrode. Moreover, by comparison with the literature in Fig. 4f, the cell performance of the PEMEC with nanoporous IrNS electrode in this study is superior to most previously reported noble metal-based OER electrodes in PEMECs up to date [33–42].

3.4. Full cell characterization of nanoporous IrNS in PEMECs with N212 membrane

To further explore the application of a nanoporous IrNS integrated electrode under high current densities of up to 6000 mA/cm^2, a thinner Nafion 212 membrane with the thickness of ~ 50 μm was applied for the cell test. The Pt/C (0.14 mg_{Pt}/cm^2) was spray coated onto the Nafion 212 membrane as cathode. As observed from the polarization curve in Fig. 5a, low cell voltages of 1.60, 1.65 and 1.78 V were obtained at the current densities of 2000, 3000 and 6000 mA/cm^2, respectively, which exceeds the U.S. Department of Energy (DOE) 2026 technical performance target (1.8 V at 3000 mA/cm^2) [43]. A stable HFR of 39 $m\Omega*cm^2$ was observed between 0 and 6000 mA/cm^2 in Fig. S5. After HFR-correction, the corresponding HFR-free cell voltages are as low as 1.53 and 1.57 V at 2000 and 6000 mA/cm^2, respectively.

Currently, various accelerated stress test (AST) protocols are still under development, and the available AST protocols in the literatures are still not able to fully correlate AST results to prediction of real-life durability in commercial PEM water electrolyzer systems. This challenge stems from the involvement of many stressors during the long-term operation conditions, such as high current density, dynamic load operation, on/off operation, temperature, water quality and differential gas pressure [44–46]. Unavoidable coupling effects between these stressors are complicated and have not been clearly understood yet. So far, stability tests of PEM water electrolyzers under constant current densities of 500–2000 mA/cm^2 have been widely reported in previous publications. In our work, we particularly chose 5000 mA/cm^2 as the main stressor to evaluate the stability of the nanoporous IrNS electrode. As seen from Fig. 5b, our stability AST protocol includes a nominal current density operation at 1800 mA/cm^2 for 90 h and a subsequent high current density operation at 5000 mA/cm^2 for 130 h. At both current densities, the nanoporous IrNS electrode displays stable performances. Notably, the degradation rate is only about 3.32 μV/h during the continuous 70-h test within the period of 150–220 h at 5000 mA/cm^2. Therefore, the developed nanoporous IrNS integrated electrode at low loadings in this work shows the potential applications for the highly efficient and robust OER under high current density

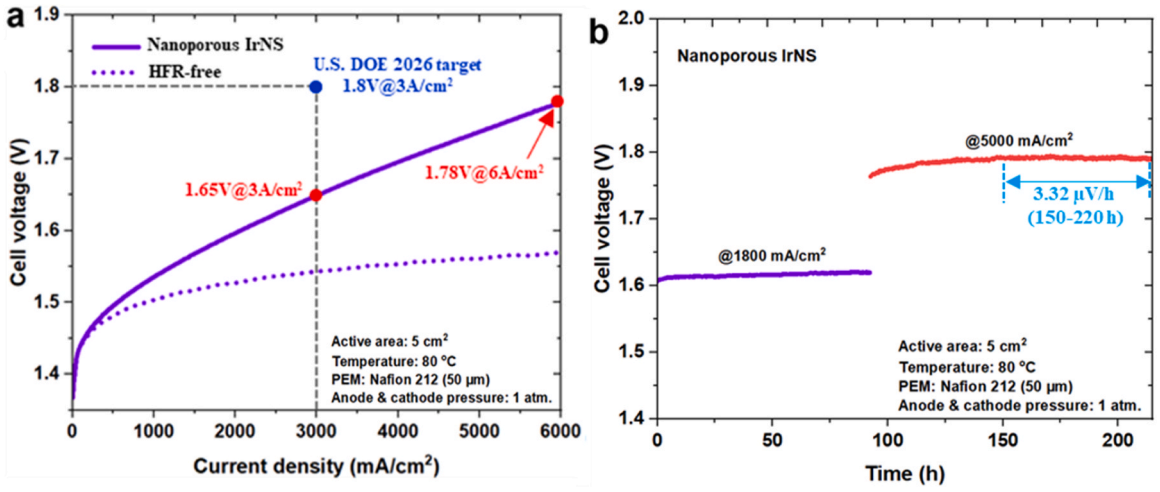

Fig. 5. (a) Polarization curves of a nanoporous IrNS integrated electrode coupled with Nafion 212 membrane under high current densities of up to 6000 mA/cm^2. (b) Cell stability tests at 1800 mA/cm^2 for 90 h and 5000 mA/cm^2 for 130 h.

operation in practical PEMECs. Except the high current density operation stressor, other stressors such as dynamic load and differential gas pressure will be incorporated in our future studies.

3.5. Post-analysis of IrNS catalysts after the electrolyzer test

The nanostructure, crystal structures and chemical compositions of IrNS catalysts after the cell durability test were analyzed by using STEM and XPS techniques. The STEM image in Fig. 6a verifies that most nanopores are remained in IrNS catalysts but the partial loss of the nanosheet structure appears after the cell durability test. The STEM image at a higher magnification in Fig. 6b shows that the tested IrNS catalysts are composed of iridium oxide nanocrystals with the tetragonal crystal structure, as evidenced by the measured lattice fringes of 0.31 and 0.27 nm, corresponding to the (110) and (101) crystal planes of iridium oxide. The (110) crystal plane for iridium oxide is further confirmed by the diffraction spots in the FFT pattern calculated from the corresponding red box in the inset of Fig. 6b. Therefore, the STEM results of as-synthesized IrNS catalysts in Fig. 3 and tested IrNS catalysts in Fig. 6 reveal that metallic IrNS catalysts before the cell test converted to iridium oxide after the stability test at 5000 mA/cm^2 in a PEM electrolzyer cell. The observed changes in nanostructure are probably attributed to the transformation from metallic iridium to iridium oxide.

The chemical composition of IrNS catalysts before and after the cell stability test was analyzed by using the XPS characterization. The high-resolution XPS spectra of Ir 4 f are presented in Fig. S6. To obtain an adequate curve-fitting, both spectra need three sets of 4 $f_{7/2}$ doublets (marked as Ir-1, Ir-2 and Ir-3), which are centered at ~62, ~63 and ~65 eV, respectively. These are tentatively assigned to Ir^{3+}, Ir^{4+} and Ir^{X+} ($X > 4$). For the as-synthesized IrNS catalysts, the iridium species with a mix of Ir^{3+}, Ir^{4+} and Ir^{X+} ($X > 4$) coexist on the catalyst surface, which is likely due to natural oxidation by air exposure. However, the metallic iridium is dominant in as-synthesized IrNS catalysts, as confirmed by the XRD analysis in Fig. 2j and STEM characterization in Fig. 3. This combination of metallic iridium with oxidized surface might improve the OER kinetics by providing good electronic conductivity and more active iridium species for the OER [47]. Compared to as-synthesized IrNS catalysts, it is found that the Ir 4 $f_{7/2}$ peak shifts towards higher binding energy after the cell stability test, which is probably attributed to the increased oxidation of catalysts during the long-term OER process. This phenomenon is consistent with previously reported studies on Ir-based OER catalysts [47–49].

4. Conclusions

In summary, we report a novel ionomer-free nanoporous iridium nanosheet electrode design, in which nanoporous iridium nanosheets with abundantly exposed edges and highly porous structures are successfully coated on TT-LGDLs by a low-temperature chemical synthesis method. The combination of high catalytic activity, good electrode electronic conductivity and excellent liquid/gas transport properties enables significantly boosted catalyst utilization and enhanced cell performance of nanoporous NS electrode. When coupled with Nafion 117 (~ 175 μm), nanoporous IrNS electrodes with low catalyst loadings can deliver the current densities of 2000 mA/cm^2 at a low cell voltage of 1.78 V, and a ~10 times higher mass specific current is achieved compared to the conventional CCM baseline at 1.8 V. Moreover, when coupled with Nafion 212 (~ 50 μm), the nanoporous IrNS electrode manifests cell voltages as low as 1.65 V and 1.78 V at 3000 and 6000 mA/cm^2, respectively. The durability test provides additional confirmation that nanoporous IrNS is capable of maintaining stable performances at both 1.8 and 5 A/cm^2 for over 200 h. Therefore, our research has revealed the beneficial effects of ionomer-free nanostructured catalysts in enhancing catalyst utilization, cell performance, and durability in PEMECs, which offers new opportunities to minimize the usage and cost of Ir-based catalysts, while accelerating the commercialization of efficient, robust and scalable PEM water electrolysis in hydrogen production.

CRediT authorship contribution statement

Zhiqiang Xie: Conceptualization, Methodology, Data curation, Writing – original draft, Writing – review & editing, Investigation, Validation. **Lei Ding:** Methodology, Investigation, Validation, Writing – review & editing. **Shule Yu:** Methodology, Investigation, Validation, Writing – review & editing. **Weitian Wang:** Investigation, Validation, Writing – review & editing. **Christopher B. Capuano:** Methodology, Investigation, Validation, Writing – review & editing. **Alex Keane:** Investigation and Validation. **Kathy Ayers:** Methodology, Investigation, Validation, Writing – review & editing. **David A. Cullen:** Conceptualization, Methodology, Resources, Investigation, Validation, Writing – review & editing. **Harry M. Meyer**: Investigation and Validation. **Feng-Yuan Zhang:** Conceptualization, Methodology, Investigation, Resources, Supervision, Project administration, Funding acquisition, Writing – review & editing.

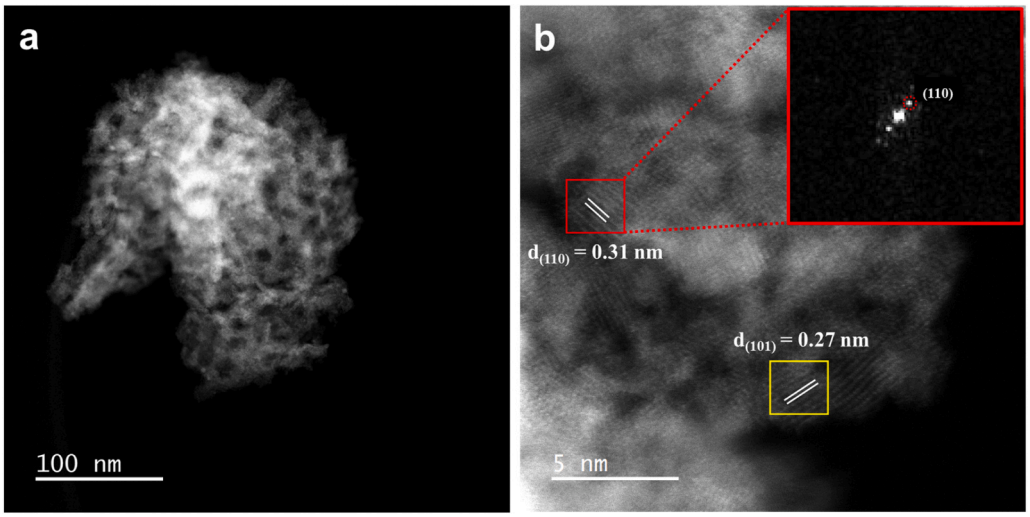

Fig. 6. (a, b) HAADF-STEM images of IrNS catalysts after the cell stability test.

Declaration of Competing Interest

The authors declare that they have no known competing financial interests or personal relationships that could have appeared to influence the work reported in this paper.

Data availability

Data will be made available on request.

Acknowledgements

The authors greatly appreciate the support from U.S. Department of Energy's Office of Energy Efficiency and Renewable Energy (EERE) under the Fuel Cell Technologies Office Award Number DE-EE0008426 and DE-EE0008423 and National Energy Technology Laboratory under Award DE-FE0011585. A portion of the research including STEM was supported by the Center for Nanophase Materials Sciences (CNMS), which is a US Department of Energy, Office of Science User Facility at Oak Ridge National Laboratory. The authors also wish to express their appreciation to Michael Koehler, Alexander Terekhov and Douglas Warnberg for their help.

Appendix A. Supporting information

Supplementary data associated with this article can be found in the online version at doi:10.1016/j.apcatb.2023.123298.

References

[1] N. Nie, D. Zhang, Z. Wang, S. Ge, Y. Gu, B. Yang, J. Lai, L. Wang, Stable p-block metals electronic perturbation in PtM@CNT (M=Ga, In, Pb and Bi) for acidic seawater hydrogen production at commercial current densities, Appl. Catal. B: Environ. 322 (2023), 122100, https://doi.org/10.1016/j.apcatb.2022.122100.

[2] B. Pivovar, N. Rustagi, S. Satyapal, Hydrogen at Scale (H 2 @Scale): key to a clean, economic, and sustainable energy system, Electrochem. Soc. Interface 27 (2018) 47–52, https://doi.org/10.1149/2.F04181if.

[3] H. Yu, N. Danilovic, Y. Wang, W. Willis, A. Poozhikunnath, L. Bonville, C. Capuano, K. Ayers, R. Maric, Nano-size IrOx catalyst of high activity and stability in PEM water electrolyzer with ultra-low iridium loading, Appl. Catal. B: Environ. 239 (2018) 133–146, https://doi.org/10.1016/j.apcatb.2018.07.064.

[4] L. Ding, K. Li, Z. Xie, G. Yang, S. Yu, W. Wang, H. Yu, J. Baxter, H.M. Meyer, D. A. Cullen, F.-Y. Zhang, Constructing ultrathin W-Doped NiFe nanosheets via facile electrosynthesis as bifunctional electrocatalysts for efficient water splitting, ACS Appl. Mater. Interfaces 13 (2021) 20070–20080, https://doi.org/10.1021/acsami.1c01815.

[5] H. Yu, L. Bonville, J. Jankovic, R. Maric, Microscopic insights on the degradation of a PEM water electrolyzer with ultra-low catalyst loading, Appl. Catal. B: Environ. 260 (2020), 118194, https://doi.org/10.1016/j.apcatb.2019.118194.

[6] Y. Wang, G. Qian, Q. Xu, H. Zhang, F. Shen, L. Luo, S. Yin, Industrially promising IrNi-FeNi3 hybrid nanosheets for overall water splitting catalysis at large current density, Appl. Catal. B: Environ. 286 (2021), 119881, https://doi.org/10.1016/j.apcatb.2021.119881.

[7] J. Mo, Z. Kang, S.T. Retterer, D.A. Cullen, T.J. Toops, J.B. Green, M.M. Mench, F.-Y. Zhang, Discovery of true electrochemical reactions for ultrahigh catalyst mass activity in water splitting, Sci. Adv. 2 (2016), e1600690, https://doi.org/10.1126/sciadv.1600690.

[8] K. Ayers, N. Danilovic, K. Harrison, H. Xu, PEM Electrolysis, a forerunner for clean hydrogen, Electrochem. Soc. Interface 30 (2021) 67, https://doi.org/10.1149/2.F16214IF.

[9] Z. Xie, S. Yu, X. Ma, K. Li, L. Ding, W. Wang, D.A. Cullen, H.M. Meyer, H. Yu, J. Tong, Z. Wu, F.-Y. Zhang, MoS2 nanosheet integrated electrodes with engineered ^{1}T–^{2}H phases and defects for efficient hydrogen production in practical PEM electrolysis, Appl. Catal. B: Environ. 313 (2022), 121458, https://doi.org/10.1016/j.apcatb.2022.121458.

[10] P. Shirvanian, F. van Berkel, Novel components in Proton Exchange Membrane (PEM) Water Electrolyzers (PEMWE): status, challenges and future needs. a mini review, Electrochem. Commun. 114 (2020), 106704, https://doi.org/10.1016/j.elecom.2020.106704.

[11] M. Bernt, C. Schramm, J. Schröter, C. Gebauer, J. Byrknes, C. Eickes, H. A. Gasteiger, Effect of the IrOx conductivity on the anode Electrode/Porous transport layer interfacial resistance in PEM water electrolyzers, J. Electrochem. Soc. 168 (2021), 084513, https://doi.org/10.1149/1945-7111/ac1eb4.

[12] K. Ayers, High efficiency PEM water electrolysis: enabled by advanced catalysts, membranes, and processes, Curr. Opin. Chem. Eng. 33 (2021), 100719, https://doi.org/10.1016/j.coche.2021.100719.

[13] C. Liu, M. Carmo, G. Bender, A. Everwand, T. Lickert, J.L. Young, T. Smolinka, D. Stolten, W. Lehnert, Performance enhancement of PEM electrolyzers through iridium-coated titanium porous transport layers, Electrochem. Commun. 97 (2018) 96–99, https://doi.org/10.1016/j.elecom.2018.10.021.

[14] M. Bernt, H.A. Gasteiger, Influence of ionomer content in IrO2/TiO2 electrodes on PEM water electrolyzer performance, J. Electrochem. Soc. 163 (2016) F3179, https://doi.org/10.1149/2.0231611jes.

[15] D. Kulkarni, A. Huynh, P. Satjaritanun, M. O'Brien, S. Shimpalee, D. Parkinson, P. Shevchenko, F. DeCarlo, N. Danilovic, K.E. Ayers, C. Capuano, I.V. Zenyuk, Elucidating effects of catalyst loadings and porous transport layer morphologies on operation of proton exchange membrane water electrolyzers, Appl. Catal. B: Environ. 308 (2022), 121213, https://doi.org/10.1016/j.apcatb.2022.121213.

[16] F.M. Sapountzi, M. Lavorenti, W. Vrijburg, S. Dimitriadou, B. Tyburska-Pueschel, P. Thüne, H. Niemantsverdriet, T.V. Pfeiffer, M.N. Tsampas, Spark ablation for the fabrication of PEM water electrolysis catalyst-coated membranes, Catalysts (2022), https://doi.org/10.3390/catal12111343.

[17] S. Higashi, A. Beniya, Ultralight conductive IrO2 nanostructured textile enables highly efficient hydrogen and oxygen evolution reaction: importance of catalyst layer sheet resistance, Appl. Catal. B: Environ. 321 (2023), 122030, https://doi.org/10.1016/j.apcatb.2022.122030.

[18] S. Choe, B.-S. Lee, M.K. Cho, H.-J. Kim, D. Henkensmeier, S.J. Yoo, J.Y. Kim, S. Y. Lee, H.S. Park, J.H. Jang, Electrodeposited IrO2/Ti electrodes as durable and cost-effective anodes in high-temperature polymer-membrane-electrolyte water electrolyzers, Appl. Catal. B: Environ. 226 (2018) 289–294, https://doi.org/10.1016/j.apcatb.2017.12.037.

[19] A. Lim, J. Kim, H.J. Lee, H.-J. Kim, S.J. Yoo, J.H. Jang, H. Young Park, Y.-E. Sung, H.S. Park, Low-loading IrO2 supported on Pt for catalysis of PEM water electrolysis and regenerative fuel cells, Appl. Catal. B: Environ. 272 (2020), 118955, https://doi.org/10.1016/j.apcatb.2020.118955.

[20] S. Yu, K. Li, W. Wang, Z. Xie, L. Ding, Z. Kang, J. Wrubel, Z. Ma, G. Bender, H. Yu, J. Baxter, D.A. Cullen, A. Keane, K. Ayers, C.B. Capuano, F.-Y. Zhang, Tuning catalyst activation and utilization via controlled electrode patterning for low-loading and high-efficiency water electrolyzers, Small 18 (2022), 2107745, https://doi.org/10.1002/smll.202107745.

[21] Z. Xie, S. Yu, G. Yang, K. Li, L. Ding, W. Wang, D.A. Cullen, H.M. Meyer, S. T. Retterer, Z. Wu, J. Sun, P.-X. Gao, F.-Y. Zhang, Ultrathin platinum nanowire based electrodes for high-efficiency hydrogen generation in practical electrolyzer cells, Chem. Eng. J. 410 (2021), 128333, https://doi.org/10.1016/j.cej.2020.128333.

[22] L. Ding, W. Wang, Z. Xie, D.S. Aaron, A. Paxson, M. Hamdan, M.M. Mench, F.-Y. Zhang, Efficient integrated electrode enables high-current operation and excellent stability for green hydrogen production, ACS Sustain. Chem. Eng. (2023), https://doi.org/10.1021/acssuschemeng.3c02083.

[23] J.H. Oh, G.H. Han, H. Kim, H.W. Jang, H.S. Park, S.Y. Kim, S.H. Ahn, Activity and stability of Ir-based gas diffusion electrode for proton exchange membrane water electrolyzer, Chem. Eng. J. 420 (2021), 127696, https://doi.org/10.1016/j.cej.2020.127696.

[24] M. Kıstı, S. Uysal, M.F. Kaya, Development of Pt coated SS316 mesh gas diffusion electrodes for a PEM water electrolyzer anode, Fuel 324 (2022), 124775, https://doi.org/10.1016/j.fuel.2022.124775.

[25] G. Yang, Z. Xie, S. Yu, K. Li, Y. Li, L. Ding, W. Wang, F.-Y. Zhang, All-in-one bipolar electrode: a new concept for compact and efficient water electrolyzers, Nano Energy 90 (2021), 106551, https://doi.org/10.1016/j.nanoen.2021.106551.

[26] Z. Kang, Y. Chen, H. Wang, S.M. Alia, B.S. Pivovar, G. Bender, Discovering and demonstrating a novel high-performing 2D-patterned electrode for proton-exchange membrane water electrolysis devices, ACS Appl. Mater. Interfaces 14 (2022) 2335–2342, https://doi.org/10.1021/acsami.1c20525.

[27] S. Chatterjee, X. Peng, S. Intikhab, G. Zeng, N.N. Kariuki, D.J. Myers, N. Danilovic, J. Snyder, Nanoporous iridium nanosheets for polymer electrolyte membrane electrolysis, Adv. Energy Mater. 11 (2021), 2101438, https://doi.org/10.1002/aenm.202101438.

[28] W. Wang, L. Ding, Z. Xie, S. Yu, B. Canfield, G. Bender, J.A. Wrubel, B.S. Pivovar, F.-Y. Zhang, Discovering reactant supply pathways at Electrode/PEM reaction interfaces via a tailored interface-visible characterization cell, Small 19 (2023), 2207809, https://doi.org/10.1002/smll.202207809.

[29] J. Mo, Z. Kang, G. Yang, S.T. Retterer, D.A. Cullen, T.J. Toops, J.B. Green, F.-Y. Zhang, Thin liquid/gas diffusion layers for high-efficiency hydrogen production from water splitting, Appl. Energy 177 (2016) 817–822, https://doi.org/10.1016/j.apenergy.2016.05.154.

[30] Z. Xie, S. Yu, G. Yang, K. Li, L. Ding, W. Wang, F.-Y. Zhang, Optimization of catalyst-coated membranes for enhancing performance in proton exchange membrane electrolyzer cells, Int. J. Hydrog. Energy (2020), https://doi.org/10.1016/j.ijhydene.2020.09.239.

[31] X. Huang, S. Tang, X. Mu, Y. Dai, G. Chen, Z. Zhou, F. Ruan, Z. Yang, N. Zheng, Freestanding palladium nanosheets with plasmonic and catalytic properties, Nat. Nanotechnol. 6 (2011) 28–32, https://doi.org/10.1038/nnano.2010.235.

[32] B. Jiang, Y. Guo, J. Kim, A.E. Whitten, K. Wood, K. Kani, A.E. Rowan, J. Henzie, Y. Yamauchi, Mesoporous metallic iridium nanosheets, J. Am. Chem. Soc. 140 (2018) 12434–12441, https://doi.org/10.1021/jacs.8b05206.

[33] J.Y. Lim, G. Rahman, S.Y. Chae, K.-Y. Lee, C.-S. Kim, O.-S. Joo, Highly stable RuO2/SnO2 nanocomposites as anode electrocatalysts in a PEM water electrolysis cell, Int. J. Energy Res. 38 (2014) 875–883, https://doi.org/10.1002/er.3081.

[34] S. Shiva Kumar, S.U.B. Ramakrishna, D. Bhagawan, V. Himabindu, Preparation of RuxPd1-xO2 electrocatalysts for the oxygen evolution reaction (OER) in PEM water electrolysis, Ionics 24 (2018) 2411–2419, https://doi.org/10.1007/s11581-017-2359-4.

[35] S.U.B. Ramakrishna, D. Srinivasulu Reddy, S. Shiva Kumar, V. Himabindu, Nitrogen doped CNTs supported Palladium electrocatalyst for hydrogen evolution reaction in PEM water electrolyser, Int. J. Hydrog. Energy 41 (2016) 20447–20454, https://doi.org/10.1016/j.ijhydene.2016.08.195.
[36] S. Shiva Kumar, S.U.B. Ramakrishna, B. Rama Devi, V. Himabindu, Phosphorus-doped carbon nanoparticles supported palladium electrocatalyst for the hydrogen evolution reaction (HER) in PEM water electrolysis, Ionics 24 (2018) 3113–3121, https://doi.org/10.1007/s11581-018-2471-0.
[37] S. Shiva Kumar, S.U.B. Ramakrishna, K. Naga Mahesh, B. Rama Devi, V. Himabindu, Palladium supported on phosphorus–nitrogen dual-doped carbon nanoparticles as cathode for hydrogen evolution in PEM water electrolyser, Ionics 25 (2019) 2615–2625, https://doi.org/10.1007/s11581-018-2783-0.
[38] T. Audichon, E. Mayousse, S. Morisset, C. Morais, C. Comminges, T.W. Napporn, K. B. Kokoh, Electroactivity of RuO2–IrO2 mixed nanocatalysts toward the oxygen evolution reaction in a water electrolyzer supplied by a solar profile, Int. J. Hydrog. Energy 39 (2014) 16785–16796, https://doi.org/10.1016/j.ijhydene.2014.07.170.
[39] F. Hegge, F. Lombeck, E. Cruz Ortiz, L. Bohn, M. von Holst, M. Kroschel, J. Hübner, M. Breitwieser, P. Strasser, S. Vierrath, Efficient and stable low iridium loaded anodes for PEM Water electrolysis made possible by nanofiber interlayers, ACS Appl. Energy Mater. 3 (2020) 8276–8284, https://doi.org/10.1021/acsaem.0c00735.
[40] M.Y. Kim, H.-J. Ban, Y.-W. Song, J. Lim, S.-J. Park, W.J. Kim, Y. Hong, B.-S. Kang, H.-S. Kim, Synthesis and electrochemical properties of nano-composite IrO2/TiO2 anode catalyst for SPE electrolysis cell, Int. J. Hydrog. Energy 47 (2022) 31098–31108, https://doi.org/10.1016/j.ijhydene.2022.07.058.
[41] G. Jiang, H. Yu, J. Hao, J. Chi, Z. Fan, D. Yao, B. Qin, Z. Shao, An effective oxygen electrode based on Ir0.6Sn0.4O2 for PEM water electrolyzers, J. Energy Chem. 39 (2019) 23–28, https://doi.org/10.1016/j.jechem.2019.01.011.
[42] E. Slavcheva, G. Borisov, E. Lefterova, E. Petkucheva, I. Boshnakova, Ebonex supported iridium as anode catalyst for PEM water electrolysis, Int. J. Hydrog. Energy 40 (2015) 11356–11361, https://doi.org/10.1016/j.ijhydene.2015.03.005.
[43] U.S. DOE Tech. Targets Proton Exch. Membr. Electro 2003.(accessed 1 May 2023).⟨https://www.energy.gov/eere/fuelcells/technical-targets-proton-exchange-membrane-electrolysis,⟩.
[44] P. Aßmann, A.S. Gago, P. Gazdzicki, K.A. Friedrich, M. Wark, Toward developing accelerated stress tests for proton exchange membrane electrolyzers, Curr. Opin. Electrochem. 21 (2020) 225–233, https://doi.org/10.1016/j.coelec.2020.02.024.
[45] C. Rakousky, U. Reimer, K. Wippermann, M. Carmo, W. Lueke, D. Stolten, An analysis of degradation phenomena in polymer electrolyte membrane water electrolysis, J. Power Sources 326 (2016) 120–128, https://doi.org/10.1016/j.jpowsour.2016.06.082.
[46] S.M. Alia, S. Stariha, R.L. Borup, Electrolyzer durability at low catalyst loading and with dynamic operation, J. Electrochem. Soc. 166 (2019) F1164, https://doi.org/10.1149/2.0231915jes.
[47] S.F. Zaccarine, M. Shviro, J.N. Weker, M.J. Dzara, J. Foster, M. Carmo, S. Pylypenko, Multi-scale multi-technique characterization approach for analysis of PEM electrolyzer catalyst layer degradation, J. Electrochem. Soc. 169 (2022), 064502, https://doi.org/10.1149/1945-7111/ac7258.
[48] F. Claudel, L. Dubau, G. Berthomé, L. Sola-Hernandez, C. Beauger, L. Piccolo, F. Maillard, Degradation mechanisms of oxygen evolution reaction electrocatalysts: a combined identical-location transmission electron microscopy and X-ray photoelectron spectroscopy study, ACS Catal. 9 (2019) 4688–4698, https://doi.org/10.1021/acscatal.9b00280.
[49] J. Feng, F. Lv, W. Zhang, P. Li, K. Wang, C. Yang, B. Wang, Y. Yang, J. Zhou, F. Lin, G.-C. Wang, S. Guo, Iridium-based multimetallic porous hollow nanocrystals for efficient overall-water-splitting catalysis, Adv. Mater. 29 (2017), 1703798, https://doi.org/10.1002/adma.201703798.